Source: Energy & Environmental Science, Vol.5, No.1, pp.5315-5324
Date of Publication: 2012-01
ISSN: 1754-5692
Publisher: Royal Society of Chemistry
DOI: 10.1039/c1ee02253a

High-Performance Quantum Dot-Sensitized Solar Cells Based on Sensitization with $CuInS_2$ Quantum Dots/CdS Heterostructure

Tzung-Luen Li,[1] Yuh-Lang Lee,[1] and Hsisheng Teng[1,2,*]

[1]Department of Chemical Engineering and Research Center for Energy Technology and Strategy, National Cheng Kung University, Tainan 70101, Taiwan

[2]Center for Micro/Nano Science and Technology, National Cheng Kung University, Tainan 70101, Taiwan

* To whom correspondence should be addressed. (E-mail): hteng@mail.ncku.edu.tw (Fax): 886-6-2344496

Abstract

A high-performance quantum dot-sensitized solar cell (QDSSC) is reported, which consists of a TiO_2/$CuInS_2$-QDs/CdS/ZnS photoanode, a polysulfide electrolyte, and a CuS counter electrode. The sensitization process involves attaching presynthesized $CuInS_2$ QDs (3.5 nm) to a TiO_2 substrate with a bifunctional linker, followed by coating CdS with successive ionic layer adsorption and reaction (SILAR) and ZnS as the last SILAR layer for passivation. This process constructs a sensitizing layer that comprises of CdS nanocrystals, closely packed around the earlier-linked $CuInS_2$ QDs, which serves as the pillars of the layer. The CuS counter electrode, prepared via successive ionic solution coating and reaction, has a small charge transfer resistance in the polysulfide electrolyte. The QDSSC exhibits a short-circuit photocurrent (J_{sc}) of 16.9 mA cm^{-2}, an open-circuit photovoltage (V_{oc}) of 0.56 V, a fill factor of 0.45, and a conversion efficiency of 4.2% under one-sun illumination. The heterojunction between the $CuInS_2$ QDs and CdS extends both the optical absorption and incident photon conversion efficiency (IPCE) spectra of the cell to a longer wavelength of approximately 800 nm, and provides an IPCE of nearly 80% at 510 nm. The high TiO_2 surface coverage of the sensitizers suppresses recombination of the photogenerated electrons. This results in a longer lifetime for the electrons, and therefore, the high V_{oc} value. The notably high J_{sc} and V_{oc} values demonstrate that this sensitization strategy, which exploits the quantum confinement reduction and other synergistic effects of the $CuInS_2$-QDs/CdS/ZnS heterostructure, can potentially outperform those of other QDSSCs.

Introduction

Based on the growing concern of global warming and the increasing demand for clean energy,[1–5] there is an urgent need to develop low-cost photovoltaic devices that can harvest photons more efficiently to achieve high power conversion efficiencies. Dye-sensitized solar cells (DSSCs) have attracted considerable attention over the past two decades in both the academic and industrial fields, and are potential low-cost photovoltaic devices with alternative structures to that of conventional silicon based solar cells. DSSCs employ a monolayer of organic-ruthenium dye molecules as the light-harvesting medium attached to a mesoscopic metal oxide film (typically anatase titanium dioxide, TiO_2), and are able to achieve power conversion efficiencies of 11.5%.[6] Instead of using molecular dyes, inorganic quantum dots (QDs) are considered as highly promising next-generation sensitizers, which possess the following advantages over dyes:[7–13] (1) easy tuning of the optical band-gap energy through controlling the QD sizes and compositions; (2) larger extinction coefficient, enabling the device thickness thinner; (3) higher stability toward water and oxygen; (4) possibilities of generating multiple excitons from single-photon absorption, through impact ionization effect (or inverse Auger process), which could push the theoretical maximum conversion efficiency of these devices as high as 44%.[14–16]

There are two common methods for assembling QDs onto TiO_2 electrodes. The first method uses presynthesized QDs, which can take advantage of the colloidal syntheses to control the growth dynamics, particle size, and crystal structure of QDs.[17–20] The second, and most common, approach utilizes the in situ preparation of QDs onto TiO_2 by successive ionic layer adsorption and reaction (SILAR)[21–27] or chemical bath deposition (CBD),[28–31] providing high surface coverage of QDs. Although various QDs such as CdS,[22,26,29] CdSe,[21,23,27,30] InP,[32] InAs,[33] Ag_2S,[34] Bi_2S_3,[16] PbS,[35] and $CuInS_2$,[36] have been investigated in the QD-sensitized solar cells (QDSSCs), their efficiencies are still considerably lower than those of DSSCs. This is a significant issue as the optimized QDSSCs configuration, including light absorption, charge

separation, hole scavenging, and charge transfer of counter electrode toward electrolytes, has not yet been acquired.[9,14]

In an earlier study we demonstrated that a photoelectrochemical system, using a photoanode consisting of a nanocrystalline TiO_2 film co-sensitized with presynthesized ternary $CuInS_2$ QDs and CdS layers, was effective in water reduction in sacrificial S^{2-}/SO_3^{2-} electrolyte under simulated solar illumination.[37] This TiO_2/$CuInS_2$-QDs/CdS photoanode exhibits superiority in incorporating the advantages of colloidal synthesis and SILAR deposition. This photoelectrode was assembled with regenerative redox couples, to survey the photovoltaic performance in a sandwich-type QDSSC. However, the most efficient iodide/triiodide (I^-/I_3^-) redox couple in DSSCs is not compatible with the commonly employed low band gap semiconducting materials, such as CdS or CdSe, due to a rapid photocorrosion process of the semiconductor. Polysulfide redox couple (S^{2-}/S_x^{2-}) is a more suitable electrolyte, compared to the alternatives, in terms of QD stability and redox activity.[21,33,38–43]

Platinum (Pt) and gold (Au), which are generally used as the counter electrode materials in DSSCs, are inefficient in S^{2-}/S_x^{2-}, as their surface activity toward interaction with the polysulfide redox couple is poor.[42] Various materials have been investigated as the counter electrode of QDSSCs, including CoS,[42,44] CuS,[44] CuS/CoS,[45] Cu_2S,[18,42,46] and carbon based fabric (nanotube,[47] graphite,[48] carbon black,[49] and mesoporous carbon[50]). Hodes et al. reported that Cu_2S acts as a suitable electrocatalyst for the S^{2-}/S_x^{2-} redox reaction.[42] Bisquert et al. fabricated CdSe QDSSC by employing different counter electrode materials, indicating that Cu_2S outperforms Au and Pt.[18] We propose a more facile route to deposit a nanocrystalline CuS layer on fluorine-doped tin oxide (FTO) transparent electrode, which exhibits an excellent electrocatalytic ability when serving as the counter electrode in the TiO_2/$CuInS_2$-QDs/CdS/ZnS QDSSCs.

This study demonstrates the potential application of co-sensitization with ternary chalcopyrite ($CuInS_2$) QDs and II–VI-compound (CdS) in QDSSC. Fig. 1a depicts the QDSSC

device configuration, and Fig. 1b is a conceptual schematic of the $CuInS_2$-QDs/CdS/ZnS heterostructure on the TiO_2 surface. The sensitization strategy is to use the $CuInS_2$ QDs (with the linkers) as the pillars, to attain an ample coverage of CdS on TiO_2. Without the pillars, the SILAR deposition may result in a CdS film with a loose particle-packing network (inset of Fig. 1b). Coating ZnS to finalize the SILAR deposition is important for passivating the light-absorbing sulfide sensitizers. Fig. 1c shows a schematic of the relative band energy levels for charge transfer in the TiO_2/$CuInS_2$-QDs/CdS/ZnS heterostructure. Due to the pronounced quantum confinement effect in the $CuInS_2$ QDs, a higher conduction band edge drives the energetics of $CuInS_2$ to more favorable levels, for electron injection from photoexcited $CuInS_2$ QDs into TiO_2.[37] The CdS coating also reduces the QD confinement, to extend the absorption spectra. By using the CuS counter electrode and polysulfide electrolyte to assemble a QDSSC, the heterostructured $CuInS_2$-QDs/CdS sensitizer provides a light-to-electrical energy conversion efficiency (η) of 4.20% under one-sun illumination and attains an incident photon to current conversion efficiency (IPCE) peak value of approximately 80%. The short-circuit photocurrent (J_{sc}) and open-circuit photovoltage (V_{oc}) achieves high values of 16.9 mA cm^{-2} and 0.56 V, respectively. A detailed characterization of the photoanode and counter electrode is presented in this study.

Experimental

Materials

Copper(I) chloride (CuCl, 99.995%), indium(III) chloride ($InCl_3$, 99.999%), 3-mercaptopropionic acid (MPA, 99+%), sodium sulfide (Na_2S, 98+%), tetramethylammonium hydroxide (97+%), titanium chloride ($TiCl_4$, 98+%), potassium chloride (KCl, 99.5%) and oleylamine (OA, 70%) were purchased from Sigma-Aldrich (USA). Cadmium nitrate (99+%)

and sulfur (99.999%) were obtained from Acros (USA). TiO_2 powder (P25, a mixed phase of 70% anatase and 30% rutile; average size 30 nm) from Degussa (Japan) was used to prepare TiO_2 anatase nanoparticles for photoelectrodes. Polyethylene glycol (PEG; 20000 in molecular weight) and ethyl cellulose from Fluka (Germany) were used to suspend TiO_2 particles in viscous solutions. Zinc nitrate ($Zn(NO_3)_2$•$6H_2O$, 99.5%) and copper(II) nitrate ($Cu(NO_3)_2$•$2.5H_2O$, 99.7%) were supplied by J. T. Baker (USA). Hexane (99.9%) and methanol (99.9%) were purchased from Tedia (USA), and ethanol (99.5%) was obtained from Merck (Germany). All the materials were used without further purification.

Preparation of CuS counter electrodes

A mask, with a window encompassed by a commercially available 3M scotch tape (810DX 3/4"), was used to define the active area of CuS electrodes (1.3 × 1.3 cm^2). 0.5 M $Cu(NO_3)_2$ methanol solution (ca. 1 mL) was first dropped on a cleaned conducting glass substrate (SnO_2:F coated glass, FTO; Hartford Glass TEC7, USA). A doctor-blade method, similar to that employed to spread the TiO_2 suspensions in DSSCs, was used to remove the excess $Cu(NO_3)_2$ solution, and to obtain a thin layer of $Cu(NO_3)_2$ on the FTO. 1 mL of 1 M Na_2S water/methanol solution (1:1 volume ratio) was uniformly dropped on the $Cu(NO_3)_2$ decorated FTO. Upon dropping, copper and sulfur ions reacted rapidly, and the color immediately changed from blue (of Cu(II)) to brown, implying the formation of the CuS. The remainder of nitrate and sodium ions, and non-reacted Na_2S and $Cu(NO_3)_2$, were rinsed away by deionized water, and then dried by an air-gun under the atmosphere conditions. The two-step dropping, rinse, and drying procedures are regarded as one deposition cycle of CuS. The incorporated amount of CuS can be increased by repeating the assembly cycles.

Preparation of Colloidal $CuInS_2$ QDs

Solvothermal synthesis was used to synthesize $CuInS_2$ QDs.[37,51] First, 0.99 mg CuCl (0.01

mmol) and 2.2 mg $InCl_3$ (0.01 mmol) were dissolved in 0.198 mL OA at room temperature. The resulting mixture was then heated to 120 °C, and maintained for 1 h with vigorous magnetic stirring, to form a clear mixture. This mixture was added, with magnetic stirring, to a Teflon-lined stainless steel autoclave (200 mL in capacity) containing 30 mL of hexane. A sulfur solution (1 mmol dissolved in 1 mL OA) was injected into the above mixture. Nucleation and subsequent growth of $CuInS_2$ QDs were carried out in a sealed autoclave at a temperature of 110 °C for 1 h. After the autoclave was cooled to room temperature, the products were washed, and centrifuged with an ethanol/methanol (1/2, v/v) solution. The resultant OA-capped QDs were dispersed in hexane for storage.

For the subsequent self-assembly of $CuInS_2$ QDs on the TiO_2 electrodes, the OA ligands on the QDs were exchanged with MPA, which is a bifunctional linker molecule containing carboxylic acid and thiol groups. In the exchange with MPA, dried OA-capped $CuInS_2$ QDs were dispersed in a methanol solution of MPA (60 mM) and tetramethylammonium hydroxide (70 mM),[50] and the mixture was then sonicated for 30 min to obtain a clear dispersion of MPA-capped $CuInS_2$ QDs. The MPA-capped QDs were precipitated by the addition of ethyl acetate/hexane (12/50, v/v) solution, and redispersed in methanol.

Fabrication of the $CuInS_2$-QDs/CdS/ZnS QDSSC

The configuration of TiO_2 on the photoanode was made of a compact underlayer, a transparent mesoporous layer (phase-pure anatase with particle size of 20 nm), and a scattering layer (ca. 400 nm) at the top. The compact layer was deposited by immersing the FTO substrate in an aqueous $TiCl_4$ solution (40 mM) at 70 °C for 30 min, followed by rinsing with deionized water and ethanol.[53] The synthesis of TiO_2 suspensions employed in the transparent, and scattering layers and the detailed procedures of constructing the mesoporous TiO_2 electrodes, are described in our previous report.[37,54,55] The thickness of the mesoporous electrodes was approximately 15 μm (11 μm of transparent layer and 4 μm of scattering layer), measured by a surface profiler of

Tencor Alpha-step 500 (USA).

The mesoporous TiO_2 electrodes were subsequently sensitized with $CuInS_2$ QDs and CdS by self-assembly and SILAR, respectively. For $CuInS_2$ QD self-assembly, the TiO_2 electrodes were heated to ~110 °C and immersed in an acetonitrile solution of MPA (1 M) and sulfuric acid (0.1 M) for 12 h.[56] Pre-treatment of MPA modification on TiO_2 surface can facilitate the $CuInS_2$ QD adsorption. The electrodes were then thoroughly rinsed with methanol before being transferred to the $CuInS_2$ QD solution. The MPA-modified TiO_2 films were left in the MPA-capped QD/methanol solution for 24 h to ensure saturated entrapment of the QDs onto the TiO_2 electrodes. For the in situ growth of CdS layers, the TiO_2/$CuInS_2$-QD electrode was successively dipped into 0.05 M $Cd(NO_3)_2$/methanol, rinsing methanol, 0.05 M Na_2S/methanol, and rinsing methanol solution. The dipping time in the Cd^{2+} and S^{2-} solution was 30 s for each, and the SILAR cycle was repeated 11 times. All the electrodes analyzed in this study have been coated with ZnS, carried out by one SILAR cycle consisting of twice dipping alternatively in the 0.2 M $Zn(NO_3)_2$ and 0.2 M Na_2S solutions for 1 min/dip. The QDSSC was assembled with the QD-sensitized photoanodes and the CuS counter electrodes, maintaining a distance of 60 μm between them by using Surlyn (Solaronix SX1170-60, Swiss) as the spacer and injecting the polysulfide electrolyte, containing 2 M Na_2S, 2 M S, and 0.2 M KCl, in the water/methanol solution (3:7 by volume). The area of the cells was 0.16 cm^2.

Measurements

Scanning electron microscopic (SEM) images were obtained using a Jeol JSM-6700F (Japan), at a beam potential of 10 kV. UV–vis absorption spectra were recorded using a Hitachi U-4100 (Japan) spectrophotometer. The crystal structure of the counter electrode samples was characterized by powder X-ray diffraction (XRD), using a Rigaku RINT-2000 (Japan) diffractometer equipped with Cu Kα radiation, excited at 40 kV and 40 mA. Transmission electron microscopy (TEM; Hitachi H-7500, Japan) and high-resolution TEM (HRTEM; FEI

Tecnai G2 F20, USA) were used to explore the microstructure of the QDs. The samples for TEM and HRTEM analysis were prepared by placing a drop of a QD solution on a carbon film-coated nickel grid, where the $CuInS_2$ QDs and the $CuInS_2$-QDs/CdS co-sensitized TiO_2 nanoparticles were dispersed in the hexane and ethanol, respectively. X-ray photoelectron spectrum (XPS) measurement was recorded with Kratos Axis Ultra DLD X-ray photoelectron spectroscope, using a monochromated Al Kα radiation at 75 W and a passing energy of 40 eV as the excitation source. The binding energies of the core levels were calibrated against C 1s binding energy set at 284.6 eV. Electrochemical impedance spectroscopy (EIS) measurements were carried out with an impedance analyzer (Zahner IM6, Germany) at zero bias potential, and an ac potential amplitude of 10 mV over the frequency range of 0.02–10^5 Hz. A symmetric configuration consisting of two identical electrodes and the polysulfide electrolyte was used in the EIS measurements.[35,57,58] Potentiostatic current–voltage polarization curves for the Pt, Au, and CuS electrodes were recorded using the Zahner IM6 analyzer in a three-electrode system with a Pt-gauze counter and an Ag/AgCl reference.

Photocurrent–voltage characteristics (*J*–*V* curves) of QDSSCs were recorded under illumination with a solar simulator (Newport, Oriel class A, SP91160A, USA) at 100 mW cm^{-2} (AM 1.5G), using an electrochemical analyzer (CH Instruments 614B, USA). The intensity of the simulated light was calibrated using a reference Si solar cell. All the measurements were conducted under ambient conditions, with no antireflective layer. Incident photon to current conversion efficiency (IPCE) of the QDSSCs was measured by DC mode method, using an IPCE analyzer (Enlitech QE-R3011, Taiwan). In the measurement of open–circuit voltage decay, samples were illuminated steadily with simulated AM 1.5G at 100 mW cm^{-2}, and the decay was studied as a function of time after the light was switched off.

Results and Discussion

Characterization of the TiO_2/$CuInS_2$-QDs/CdS/ZnS electrode

Fig. 2a shows the transmission electron microscopy (TEM) image of the $CuInS_2$ QDs used in TiO_2 sensitization. The particle size was 3.5 ± 0.4 nm. The inset of Fig. 2a shows that the oleylamine-capped $CuInS_2$/hexane dispersion has an orange color, indicating absorption of a great proportion of visible light. Fig. 2b shows the TEM image of TiO_2 nanoparticles, co-sensitized with $CuInS_2$-QDs/CdS. The sensitizers sufficiently cover the nanocrystalline TiO_2 network with a thickness of 5–8 nm. The high-resolution TEM (HRTEM) image of the TiO_2/$CuInS_2$-QDs/CdS composite (Fig. 2c) clearly depicts the crystalline lattice fringes of the involved species. The lattice spacing distance of 0.351 nm, illustrated in the right zone of the image, corresponds to the (101) plane of anatase TiO_2. The lattices with spacing distances of 0.320 and 0.335 nm around the TiO_2 particle correspond to the (112) plane of the tetragonal $CuInS_2$ (JCPDS file no. 85–1575) and (111) plane of the cubic CdS (JCPDS file no. 80–0019), respectively. The CdS coating by SILAR has a polycrystalline structure (encompassed by yellow lines), and is in close contact with both the $CuInS_2$ QDs (encompassed by red lines) and TiO_2 particles.

Fig. 3 shows the absorption spectra of the naked TiO_2 film, and the TiO_2 films sensitized with $CuInS_2$ QDs, CdS or $CuInS_2$-QDs/CdS. The naked TiO_2 film absorbs only UV light (wavelengths of <420 nm). After sensitization the absorption spectra of the TiO_2 films extend to the visible light region. The absorption of the TiO_2/$CuInS_2$ electrode occurs at approximately 650 nm, by a distinct blue-shift relative to that of bulk $CuInS_2$ (ca. 830 nm).[59] The absorption onset for the TiO_2/CdS occurs at approximately 580 nm. The TiO_2/$CuInS_2$-QDs/CdS electrode exhibits a red-shifted absorption onset at approximately 780 nm after CdS coating. As the CdS layer has an absorption onset at 580 nm, the red-shift must result from the light absorption of the $CuInS_2$ QDs. This red-shift may indicate that the QD charge carrier wave functions tunnel into the surrounding CdS shell, as the conduction and valence band edge levels of $CuInS_2$ QDs and

CdS are close,[59,60] thereby reducing the confinement energy, resulting in a red-shift in the absorption spectra.

In the photovoltaic performance assessment, the co-sensitized TiO_2/$CuInS_2$-QDs/CdS photoelectrodes (coated with a final ZnS layer) were incorporated with a polysulfide electrolyte, and a Pt or Au counter electrode, to form sandwich-type QDSSCs. The performance was poor because the charge transfer efficiency (or the electrocatalytic activity) of Pt or Au in the polysulfide electrolyte was unsatisfactory (see Figs. S1 and S2 of the ESI†).[18,57] To improve the activity of the counter electrode, a nanocrystalline CuS film was deposited on the FTO substrate to replace the Pt and Au deposits.

Development of the CuS counter electrode

Successive ionic solution coating and reaction (SISCR) deposition was used to deposit CuS films as the counter electrode, and the growth mechanism of the CuS nanocrystals was monitored with scanning electron microscopy (see Fig. S3 of the ESI†). Complete coverage of the FTO substrate by a CuS layer, which consists of nanoparticles of 30–80 nm in size, can be obtained by increasing the deposition cycle to 4. The copper–sulfur aqueous chemistry is complex, as several stable and metastable phases of varying stoichiometries exist between ideal compositions of Cu_2S and CuS.[61,62] Fig. 4 illustrates the XRD pattern of the nanocrystalline CuS layer from 4 cycle SISCR deposition. The main diffraction peaks are identical to those of the hexagonal phase CuS (JCPDS file no. 79-2321), justifying the formation of CuS nanocrystals from SISCR. The Cu ion of the sample is identified to be in the CuS state by using XPS (see Fig. S4 of the ESI†).[63–66] Both XRD and XPS analyses confirm that the films obtained from SILAR deposition are nanocrystalline CuS.

The CuS electrodes were subjected to analysis with EIS for charge transfer resistance (R_{ct}) values in the polysulfide electrolyte (see Fig. S5 of the ESI†). The R_{ct} between the electrode and the polysulfide electrolyte decreases with increasing deposition cycles, and after 4 deposition

cycles, becomes stabilized at 4.2 Ω cm^2. In comparison to the Pt and Au electrodes, the CuS electrodes exhibited a significantly lower R_{ct} for interaction with the polysulfide electrolyte. Fan et al. fabricated ordered multimodal porous carbon (OMPC) to serve as the counter electrode in CdS/CdSe-based QDSSCs, and due to the unique ordered hierarchical nanostructure, demonstrated very low R_{ct} toward the polysulfide electrolyte (3.5 Ω cm^2) for the OMPC electrode.[58] However, Nernst diffusion impedance of the electrolyte appeared in the corresponding impedance spectra, due to the porous framework of the OMPC electrode. The CuS electrodes, developed in this study, have comparably low R_{ct} values, and do not display any perceivable pore diffusion impedance for the electrolyte.

Fig. 5 shows the potentiostatic current–voltage polarization curves of the Pt, Au, and the CuS electrodes in the polysulfide electrolyte. The current induced by polarization directly gives the electrocatalytic activity of the electrodes. The polarization measurements show that the CuS electrodes outperform the Pt and Au electrodes in the polysulfide electrolyte. As to the effect of CuS deposition cycle number, the 4-cycle SISCR CuS electrode has the highest polarization current, in accord with the R_{ct} results obtained from EIS. Therefore, based on the current–voltage polarization curve and EIS measurements, it is viable to use the CuS electrodes as the counter for QDSSCs, to replace conventional Pt or Au electrodes.

Performance of QDSSCs based on CuS counter electrodes

Fig. 6 shows the photocurrent–voltage characteristics (*J*–*V* curves) of the QDSSCs, using CuS electrodes of varying SISCR cycles as the counter electrode. In comparison to the results of using the Pt and Au electrodes (Fig. S1 of the ESI†), the CuS electrodes significantly improved the photocurrent and open-circuit voltage of QDSSCs. The photocurrent increases with each CuS deposition cycle, and reaches a maximum at 4 cycles; therefore, further deposition does not increase the photocurrent. The photocurrent variation conforms to the trend of R_{ct} (Fig. S5 of the ESI†) and polarization current (Fig. 5) for the counter electrodes. Table 1 summarizes the

performance indices of the cells, based on the data of Fig. 6. Both J_{sc} and *FF* increase with each deposition cycle, and reach a maximum at 4 cycles, whereas V_{oc} remains relatively invariant. The QDSSCs can reach a η maximum of 4.20%, primarily due to the increase in J_{sc} and *FF*. The above results indicate that the R_{ct} (or the electrocatalytic activity) of the counter electrodes governs the J_{sc} and *FF* values, and therefore the conversion efficiency of the QDSSCs. The CuS counter electrodes achieved an *FF* value of 0.45, while Pt or Au produced a value of ~0.3 (Fig. S1 of the ESI†). However, a QDSSC assembled with CuS-based counter electrodes has the potential to obtain an even higher *FF* value, via modification of the CuS structure or deposition method.[45] Further studies are planned, along with a more detailed investigation into the correlation between the structure of CuS-based electrode and the *FF* value. As the SISCR deposition of 4 cycles is the optimal process for CuS counter electrodes, the following discussion on the synergistic effects considers only the QDSSCs assembled with the 4-cycle CuS electrode.

Synergistic effects of $CuInS_2$-QDs/CdS co-sensitization

Fig. 7 shows the comparison of the *J–V* characteristics for the $CuInS_2$ QDs-, CdS-, and $CuInS_2$-QDs/CdS-sensitized cells that were incorporated with the 4-cycle CuS electrode. The data for the $CuInS_2$-QDs/CdS-sensitized cell are extracted from Fig. 6 for comparison. Table 1 also lists the performance indices of the $CuInS_2$ QDs- and CdS-sensitized cells. The cells that were sensitized with individual $CuInS_2$ QDs or CdS are inferior in performance to the cell co-sensitized with $CuInS_2$-QDs/CdS. The J_{sc} value was 16.9 mA cm^{-2} for the $CuInS_2$-QDs/CdS-sensitized cell, whereas the values were 1.56 and 8.06 mA cm^{-2} for the $CuInS_2$ QDs- and CdS-sensitized cells, respectively. The lower J_{sc} of the $CuInS_2$ QDs cell, relative to that of the CdS cell, can be attributed to the sparser QDs coverage on the TiO_2 surface and the more defected surface of the QDs. Fig. 3 illustrates that the TiO_2/CdS electrode exhibits a stronger optical absorption spectrum than the TiO_2/$CuInS_2$-QDs. Denser sensitizer coverage

not only absorbs more incident photons, but also inhibits recombination of photogenerated charges with the electrolyte. Previous studies reported that SILAR deposition can form a closely-packed layer on TiO_2 surface, while using a bifunctional linker to attach QDs results in low surface coverage.[14,67] Coating CdS on the TiO_2/$CuInS_2$-QDs surface prominently improved the J_{sc} to 16.9 mA cm^{-2}, a value comparable to that of ruthenium dye-based DSSCs.

In the $CuInS_2$-QDs/CdS-sensitized cell, the CdS sensitizer's contribution to J_{sc} should be no more than the J_{sc} value of the CdS-sensitized cell (8.06 mA cm^{-2}). This indicates that the contribution from the CdS-coated $CuInS_2$ QDs is at least 8.84 mA cm^{-2} (= 16.9 mA cm^{-2} – 8.06 mA cm^{-2}). The $CuInS_2$ QDs-sensitized cell had a low J_{sc} value of 1.56 mA cm^{-2}, and the CdS coating prominently increased the J_{sc} value of $CuInS_2$ QDs to 8.84 mA cm^{-2}. The extended absorption spectrum (Fig. 3), caused by quantum confinement reduction with CdS coating, should have contributed to the photocurrent increase, but cannot account for the entire enhancement as the photon absorption increase was not as high as the photocurrent increase. Thus, the CdS coating may have passivated the QDs' surface and suppressed the charge recombination or the electron leakage to the electrolyte. The role of CdS in surface passivation of the $CuInS_2$ QDs may be one of the critical mechanisms for enhancing the J_{sc} value. Note that the final coating of ZnS on the photoelectrodes is essential because it passivates the CdS layer and promotes the cell performance (see Fig. S6 of the ESI† for the *J*–*V* characteristics of the $CuInS_2$-QDs/CdS-sensitized cell without ZnS coating).

To clarify how the absorption spectrum widening and surface passivation effects, resulting from co-sensitizatio ton, can affect the quantum efficiency, we subjected the cells to IPCE analysis at varying excitation wavelengths. The IPCE characteristics of the cells (Fig. 8) are consistent to their absorption spectra (Fig. 3). The IPCE value increases significantly with co-sensitization, and the IPCE value of the co-sensitized cell is larger than the IPCE sum total of the other two cells. This proves that the surface passivation mechanism promotes the charge injection into TiO_2. The $CuInS_2$-QDs/CdS cell has a maximum IPCE of 78% at 510 nm,

whereas the maximum IPCE values were only 17% for the $CuInS_2$ QDs cell at 360 nm, and 43% for the CdS cell at 450 nm. An IPCE value of approximately 80% is one of the highest IPCE values obtained for QDSSCs.[18,20,45,72] The co-sensitization extends the IPCE response spectrum from 600 nm or less (for the cells with individual $CuInS_2$ QDs or CdS) to 800 nm or above. Although the IPCE values are considerably lower at wavelengths near 800 nm, the wide photon conversion spectrum, which has higher IPCE values than that of typical CdS/CdSe-sensitized QDSSCs at wavelengths above 700 nm,[23,73] can explain the high J_{sc} of 16.9 mA cm^{-2} achieved in this study. The contribution to IPCE at longer wavelengths arises from the light absorption of $CuInS_2$ QDs, and not CdS, as CdS is not photoactive to the photons with smaller energy. This demonstrates the occurrence of reduction of the quantum confinement in the $CuInS_2$ QDs, as observed in the absorption spectra (Fig. 3).

This study also estimated the short-circuit photocurrents from the integrated IPCE spectra (Fig. 8) and obtained values of 4.1 and 13 mA cm^{-2} for the CdS- and $CuInS_2$-QDs/CdS-sensitized cells. These short-circuit photocurrents are smaller than the J_{sc} values obtained from the *J*–*V* measurements under one-sun (AM 1.5G) illumination (Fig. 7). The discrepancy can be attributed to the highly defected feature of the $CuInS_2$-QDs and CdS deposited on TiO_2. In the IPCE measurements the monochromatic light intensities were much lower than that of AM 1.5G illumination and charge separation and collection are more efficient at high illumination intensities.[4,45] This effect is especially significant for the CdS-sensitized cell at wavelengths longer than 550 nm as the IPCE result shows negligibly small values while the absorption is rather active.

In addition to enhancing J_{sc}, Fig. 7 shows that coating CdS on the TiO_2/$CuInS_2$-QDs electrode significantly increases V_{oc}. The V_{oc} values for different sensitizers show an order of $CuInS_2$ QDs(0.354 V) < CdS(0.490 V) < $CuInS_2$-QDs/CdS(0.560 V). The V_{oc} value is closely related to the recombination of charges at the TiO_2 surface. Fig. 9 shows the dark current–voltage curves for the cells. The dark current onset voltage had an order identical to that

for the V_{oc} value. This confirms that charge recombination on TiO_2 influences the V_{oc} value. SILAR deposition of CdS can provide a higher TiO_2 surface coverage than $CuInS_2$ QDs, and the CdS-sensitized cell shows a higher dark current onset voltage than the $CuInS_2$ QDs-sensitized cell. The $CuInS_2$-QDs/CdS-sensitized cell had a higher dark current onset voltage than that of the CdS cell, indicating that the TiO_2 surface coverage of the former is higher. The result suggests that the first linked $CuInS_2$ QDs may have increased the TiO_2 surface energy (by increasing the surface roughness) to improve the degree of CdS attachment on the surface. Fig. 1b shows the conceptual schematic of the sensitizer nanoarchitecture, in which CdS nanocrystals are closely packed around the linked $CuInS_2$ QD pillars. Without the pillars, the CdS formed by SILAR shows a loose packing network that is less resistant to recombination. This surface covering strategy resulted in an insulated TiO_2 surface, and therefore a high V_{oc} value for the consequent cell.

To further explore the recombination mechanism on the photoelectrode, the cells were subjected to open-circuit voltage decay analysis, which can obtain the time that the electrons reserve in the conduction band of TiO_2 (that is, the lifetime τ_n). Fig. 10a shows the variation of V_{oc} with time for the cells illuminated to a steady state voltage, with subsequent interruption of illumination. The voltage decay with time gives the electron lifetime according to[74,75]

$$\tau_n = -\frac{k_B T}{e}\left(\frac{dV_{oc}}{dt}\right)^{-1} \qquad (1)$$

where k_B is the Boltzmann constant (1.38×10^{-23} J K^{-1}), T is the absolute temperature (298 K), and e is the electronic charge (1.602×10^{-19} C). Fig. 10b shows the electron lifetime obtained from the voltage decay results. The electron lifetime of all the cells increases with the decreasing V_{oc}. The lifetime spans two orders of magnitude, from 0.2 to 50 s. At the same V_{oc} values, the lifetimes of the cells with different sensitizers have an order of $CuInS_2$-QDs/CdS > CdS > $CuInS_2$ QDs. The longer lifetime of the $CuInS_2$-QDs/CdS co-sensitized cell confirms that the ample coverage of the $CuInS_2$-QDs/CdS heterostructure suppressed the recombination of

photogenerated electrons in the TiO_2 film with electrolyte.

Conclusions

A QDSSC assembled with a TiO_2/$CuInS_2$-QDs/CdS/ZnS photoanode and a CuS counter electrode results in a J_{sc} of 16.9 mA cm^{-2}, V_{oc} of 0.56 V, and η of 4.20% under one-sun illumination. The TiO_2 sensitization strategy, which includes attaching $CuInS_2$ QDs with a bifunctional linker followed by SILAR coating of CdS, constructs a structured sensitizing layer that consists of CdS nanocrystals closely packed around the earlier-linked $CuInS_2$ QDs, which serve as the pillars of the layer. The heterojuction between CdS and $CuInS_2$ resulted in reduction of quantum confinement in the $CuInS_2$ QDs, and therefore extended the optical absorption spectrum. The CdS coating may also play a role in surface passivation of the $CuInS_2$ QDs, to suppress the recombination of photogenerated charges. Due to the quantum confinement reduction and surface passivation effects, the $CuInS_2$-QDs/CdS-sensitized cell showed a wide IPCE action spectrum (ranging to 800 nm), and a peak conversion efficiency of nearly 80% at 510 nm. These synergistic effects of co-sensitization, along with the high electrocatalytic activity of the CuS counter electrode, resulted in the high J_{sc} value of the cell. The intimate coverage of CdS on TiO_2 surface reduces the recombination of photogenerated electrons with electrolyte, and thus increases the V_{oc} value. This study presents a sensitization strategy that simultaneously exploits the benefits of semiconductor heterojunction and creates an intimate coverage on TiO_2 surface for high J_{sc} and V_{oc} values. By a further reduction of the series resistance of cells for higher *FF* values, this sensitization strategy has the potential of advancing the QDSSC performance to a level comparable to that of DSSCs.

Acknowledgment

This research is supported by the National Science Council of Taiwan (100-3113-E-007-008 and 98-2221-E-006-112-MY2), and the Bureau of Energy, Ministry of Economic Affairs, Taiwan (100-D0204-2).

† **Electronic supplementary information (ESI) available:** The *J*–*V* curves of QDSSCs assembled with the TiO_2/$CuInS_2$-QDs/CdS/ZnS photoanode and Pt or Au counter electrodes under one-sun illumination; Nyquist impedance plots of Au and Pt electrodes in the polysulfide electrolyte; SEM images of the CuS nanocrystalline films deposited with varying SISCR cycles; Cu 2p XPS spectra of the CuS film; Nyquist impedance plots of the CuS electrodes in the polysulfile electrolyte; the *J*–*V* curves of a QDSSC assembled with a $CuInS_2$-QDs/CdS-sensitized photoanode without ZnS coating, and the 4-cycle SISCR CuS counter electrode under one-sun illumination.

References

1 P. V. Kamat, *J. Phys. Chem. C*, 2007, **111**, 2834–2860.

2 T. F. Yeh, J. M. Syu, C. Cheng, T. H. Chang and H. Teng, *Adv. Funct. Mater.*, 2010, **20**, 2255–2262.

3 C. C. Hu and H. Teng, *J. Phys. Chem. C*, 2010, **114**, 20100–20106.

4 K. P. Wang and H. Teng, *Phys. Chem. Chem. Phys.*, 2009, **11**, 9489–9496.

5 P. T. Hsiao, M. D. Lu, Y. L. Tung and H. Teng, *J. Phys. Chem. C*, 2010, **114**, 15625−15632.

6 C.-Y. Chen, M. Wang, J.-Y. Li, N. Pootrakulchote, L. Alibabaei, C. Ngoc-le, J. D. Decoppet, J.-H. Tsai, C. Grätzel, C.-G. Wu, S. M. Zakeeruddin and M. Grätzel, *ACS Nano*, 2009, **3**, 3103−3109.

7 A. J. Nozik, *Physica E*, 2002, **14**, 115−120.

8 P. V. Kamat, *J. Phys. Chem. C*, 2008, **112**, 18737−18753.

9 G. Hodes, *J. Phys. Chem. C*, 2008, **112**, 17778−17787.

10 W. U. Huynh, J. J. Dittmer and A. P. Alivisatos, *Science*, 2002, **295**, 2425−2427.

11 R. D. Schaller and V. I. Klimov, *Phys. Rev. Lett.*, 2004, **92**, 186601.

12 M. Shalom, I. Hod, Z. Tachan, S. Buhbut, S. Tirosh and A. Zaban, *Energy Environ. Sci.*, 2011, **4**, 1874−1878.

13 S. H. Im, H. J. Kim, S. W. Kim, S. W. Kim and S. I. Seok, *Energy Environ. Sci.*, 2011, advance article, DOI: 10.1039/C1EE01774H.

14 I. Mora-Seró, S. Giménez, F. Fabregat-Santiago, R. Gómez, Q. Shen, T. Toyoda and J. Bisquert, *Acc. Chem. Res.*, 2009, **42**, 1848−1857.

15 S. Buhbut, S. Itzhakov, E. Tauber, M. Shalom, I. Hod, T. Geiger, Y. Garini, D. Oron and A. Zaban, *ACS Nano*, 2010, **4**, 1293−1298.

16 L. M. Peter, K. G. U. Wijayantha, D. J. Riley and J. P. Waggett, *J. Phys. Chem. B*, 2003, **107**, 8378−8381.

17 J. H. Bang and P. V. Kamat, *ACS Nano*, 2009, **3**, 1467–1476.

18 S. Giménez, I. Mora-Seró, L. Macor, N. Guijarro, T. Lana-Villarreal, R. Gómez, L. J. Diguna, Q. Shen, T. Toyoda and J. Bisquert, *Nanotechnology*, 2009, **20**, 295204.

19 N. Guijarro, T. Lana-Villarreal, I. Mora-Seró, J. Bisquert and R. Gómez, *J. Phys. Chem. C*, 2009, **113**, 4208–4214.

20 A. Salant, M. Shalom, I. Hod, A. Faust, A. Zaban and U. Banin, *ACS Nano*, 2010, **4**, 5962–5968.

21 H. Lee, M. K. Wang, P. Chen, D. R. Gamelin, S. M. Zakeeruddin, M. Grätzel and M. K. Nazeeruddin, *Nano Lett.*, 2009, **9**, 4221–4227.

22 C. H. Chang and Y. L. Lee, *Appl. Phys. Lett.*, 2007, **91**, 053503.

23 Y. L. Lee and Y. S. Lo, *Adv. Funct. Mater.*, 2009, **19**, 604–609.

24 D. R. Baker and P. V. Kamat, *Adv. Funct. Mater.*, 2009, **19**, 805–811.

25 H. M. Pathan and C. D. Lokhande, *Bull. Mater. Sci.*, 2004, **27**, 85–111.

26 R. Vogel, K. Pohl and H. Weller, *Chem. Phys. Lett.*, 1990, **174**, 241–245.

27 Q. Shen, J. Kobayashi, L. J. Diguna and T. Toyoda, *J. Appl. Phys.*, 2008, **103**, 084304.

28 S. Gorer and G. Hodes, *J. Phys. Chem.*, 1994, **98**, 5338–5346.

29 M. Shalom, S. Dor, S. Ruhle, L. Grinis and A. Zaban, *J. Phys. Chem. C*, 2009, **113**, 3895–3898.

30 L. J. Diguna, Q. Shen, J. Kobayashi and T. Toyoda, *Appl. Phys. Lett.*, 2007, **91**, 023116.

31 M. Shalom, S. Ruhle, I. Hod, S. Yahav and A. Zaban, *J. Am. Chem. Soc.*, 2009, **131**, 9876–9877.

32 A. Zaban, O. I. Mićić, B. A. Gregg and A. J. Nozik, *Langmuir*, 1998, **14**, 3153–3156.

33 P. Yu, K. Zhu, A. G. Norman, S. Ferrere, A. J. Frank and A. J. Nozik, *J. Phys. Chem. B*, 2006, **110**, 25451–25454.

34 A. Tubtimtae, K. L. Wu, H. Y. Tung, M. W. Lee and G. J. Wang, *Electrochem. Commun.*, 2010, **12**, 1158–1160.

35 H. J. Lee, P. Chen, S.-J. Moon, F. Sauvage, K. Sivula, T. Bessho, D. R. Gamelin, P. Comte,

S. M. Zakeeruddin, S. Il Seok, M. Grätzel and M. K. Nazeeruddin, *Langmuir*, 2009, **25**, 7602–7608.

36 K. T. Kuo, D. M. Liu, S. Y. Chen and C. C. Lin, *J. Mater. Chem.*, 2009, **19**, 6780–6788.

37 T. L. Li, Y. L. Lee and H. Teng, *J. Mater. Chem.*, 2011, **21**, 5089–5098.

38 S. A. Sapp, C. M. Elliott, C. Contado, S. Caramori and C. A. Bignozzi, *J. Am. Chem. Soc.*, 2002, **124**, 11215–11222.

39 H. J. Lee, J.-H. Yum, H. C. Leventis, S. M. Zakeeruddin, S. A. Haque, P. Chen, S. Il Seok, M. Grätzel and M. K. Nazeeruddin, *J. Phys. Chem. C*, 2008, **112**, 11600–11608.

40 Y. Tachibana, H. Y. Akiyama, Y. Ohtsuka, T. Torimoto and S. Kuwabata, *Chem. Lett.*, 2007, **36**, 88–89.

41 L. Li, X. Yang, J. Gao, H. Tian, J. Zhao, A. Hagfeldt and L. Sun, *J. Am. Chem. Soc.*, 2011, **133**, 8458–8460.

42 G. Hodes, J. Manassen and D. Cahen, *J. Electrochem. Soc.*, 1980, **127**, 544–549.

43 B. Miller and A. Heller, *Nature*, 1976, **262**, 680–681.

44 Z. Yang, C. Y. Chen, C. W. Liu and H. T. Chang, *Chem. Commun.*, 2010, **46**, 5485–5487.

45 Z. Yang, C. Y. Chen, C. W. Liu, C. L. Li and H. T. Chang, *Adv. Energy Mater.*, 2011, **1**, 259–264.

46 V. González-Pedro, X. Xu, I. Mora-Seró and J. Bisquert, *ACS Nano*, 2010, **4**, 5783–5790.

47 S.-R. Jang, R. Vittal and K.-J. Kim, *Langmuir*, 2004, **20**, 9807–9810.

48 K. Imoto, K. Takahashi, T. Yamaguchi, T. Komura, J. Nakamura and K. Murata, *Sol. Energy Mater. Sol. Cells*, 2003, **79**, 459–469.

49 T. N. Murakami, S. Ito, Q. Wang, M. K. Nazeeruddin, T. Bessho, I. Cesar, P. Liska, R. Humphry-Baker, P. Comte, P. Pechy and M. Grätzel, *J. Electrochem. Soc.*, 2006, **153**, A2255–A2261.

50 B. Fang, S.-Q. Fan, J. H. Kim, M.-S. Kim, M. Kim, N. K. Chaudhari, J. Ko and J.-S. Yu, *Langmuir*, 2010, **26**, 11238–11243.

51 T. L. Li and H. Teng, *J. Mater. Chem.*, 2010, **20**, 3656–3664.

52 K. S. Leschkies, R. Divakar, J. Basu, E. Enache-Pommer, J. E. Boercker, C. B. Carter, U. R. Kortshagen, D. J. Norris and E. S. Aydil, *Nano Lett.*, 2007, **7**, 1793–1798.

53 S. Ito, P. Chen, P. Comte, M. K. Nazeeruddin, P. Liska, P. Péchy and M. Grätzel, *Progr. Photovolt.: Res. Appl.*, 2007, **15**, 603–612.

54 P. T. Hsiao, K. P. Wang, C. W. Cheng and H. Teng, *J. Photochem. Photobiol. A*, 2007, **188**, 19–24.

55 C. C. Tsai and H. Teng, *Chem. Mater.*, 2006, **18**, 367–373.

56 A. Kongkanand, K. Tvrdy, K. Takechi, M. Kuno and P. V. Kamat, *J. Am. Chem. Soc.*, 2008, **130**, 4007–4015.

57 S.-Q. Fan, B. Fang, J. H. Kim, J.-J. Kim, J.-S. Yu and J. Ko, *Appl. Phys. Lett.*, 2010, **96**, 063501.

58 S.-Q. Fan, B. Fang, J. H. Kim, B. Jeong, C. Kim, J.-S. Yu and J. Ko, *Langmuir*, 2010, **26**, 13644–13649

59 S. B. Zhang, S.-H. Wei and A. Zunger, *J. Appl. Phys.*, 1998, **83**, 3192–3196.

60 R. Vogel, P. Hoyer and H. Weller, *J. Phys. Chem.*, 1994, **98**, 3183–3188.

61 R. H. Kore, J. S. Kulkarni and S. K. Haram, *Chem. Mater.*, 2001, **13**, 1789–1793.

62 M. Orphanou, E. Leontidis, T. K. Leodidou, P. Koutsoukos and K. C. Kyriacou, *Langmuir*, 2004, **20**, 5605–5612.

63 A. Tang, S. Qu, K. Li, Y. Hou, F. Teng, J. Cao, Y. Wang and Z. Wang, *Nanotechnology*, 2010, **21**, 285602.

64 M. Sam, M. R. Bayati, M. Mojtahedi and K. Janghorban, *Appl. Surf. Sci.*, 2010, **257**, 1449–1453.

65 C. D. Wagner, *Discuss. Faraday Soc.*, 1975, **60**, 291–300.

66 L. Chen, J. Chen, H. Zhou, L. Liu and H. Wan, *Mater. Lett.*, 2007, **61**, 1974–1977.

67 I. Mora-Seró, V. Likodimos, S. Giménez, E. Martínez-Ferrero, J. Albero, E. Palomares, A.

G. Kontos, P. Falaras and J. Bisquert, *J. Phys. Chem. C*, 2010, **114**, 6755–6761.

68 N. Serpone, E. Borgarello and M. Grätzel, *J. Chem. Soc., Chem. Commun.*, 1984, 342–344.

69 N. Serpone, P. Maruthamuthu, P. Pichat, E. Pelizzetti and H. Hidaka, *J. Photochem. Photobiol. A*, 1995, **85**, 247–255.

70 C. C. Hu, J. N. Nian and H. Teng, *Sol. Energy Mater. Sol. Cells*, 2008, **92**, 1071–1076.

71 Y. Sasaki, H. Nemoto, K. Saito and A. Kudo, *J. Phys. Chem. C*, 2009, **113**, 17536–17542.

72 Q. Zhang, X. Guo, X. Huang, S. Huang, D. Li, Y. Luo, Q. Shen, T. Toyoda and Q. Meng, *Phys. Chem. Chem. Phys.*, 2011, **13**, 4659–4667.

73 H. J. Lee, J. Bang, J. Park, S. Kim and S.-M. Park, *Chem. Mater.*, 2010, **22**, 5636–5643.

74 P. T. Hsiao and H. Teng, *J. Taiwan Inst. Chem. Eng.*, 2010, **41**, 676–681.

75 Z. Liu, M. Miyauchi, Y. Uemura, Y. Cui, K. Hara, Z. Zhao, K. Sunahara and A. Furube, *Appl. Phys. Lett.*, 2010, **96**, 233107.

Table 1. Photovoltaic parameters obtained from photocurrent–voltage characteristics of QDSSCs assembled with the $CuInS_2$-QDs/CdS-sensitized photoanode having a final ZnS coating and the CuS counter electrodes from varying SISCR cycles (upper pannel) and QDSSCs assembled with the 4-cycle SISCR counter electrode and various photoanodes sensitized with individual $CuInS_2$ QDs or CdS, also having a final ZnS coating (lower pannel).

photoanode	counter	V_{oc} (V)	J_{sc} (mA cm^{-2})	*FF*	η (%)
$CuInS_2$-QDs/CdS	CuS_1	0.575	13.6	0.36	2.83
$CuInS_2$-QDs/CdS	CuS_2	0.568	15.2	0.41	3.52
$CuInS_2$-QDs/CdS	CuS_3	0.564	16.3	0.41	3.83
$CuInS_2$-QDs/CdS	CuS_4	0.560	16.9	0.45	4.20
$CuInS_2$-QDs/CdS	CuS_5	0.560	17.0	0.44	4.15
$CuInS_2$ QDs	CuS_4	0.354	1.56	0.56	0.31
CdS	CuS_4	0.490	8.06	0.46	1.80

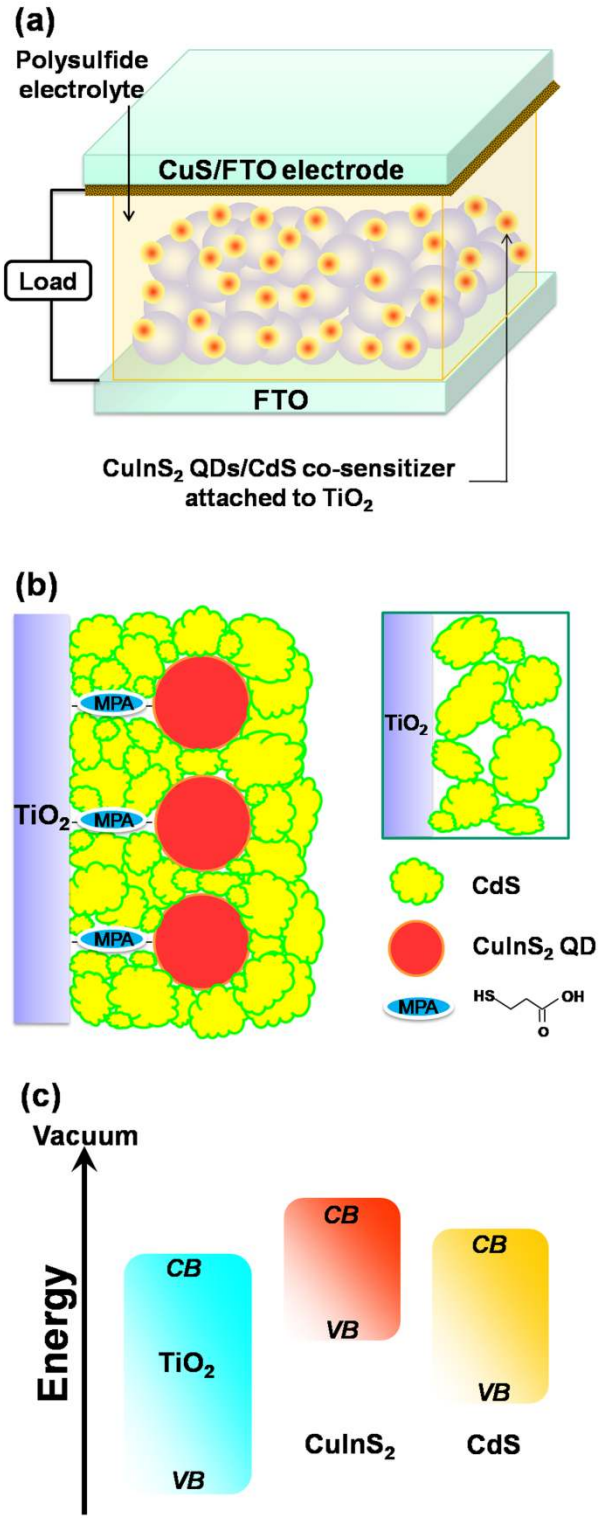

Fig. 1. (a) Schematic illustration of the quantum dot-sensitized solar cell, which consists of a TiO_2 nanocrystalline film sensitized with $CuInS_2$-QDs/CdS as the photoanode, a CuS film, deposited on a SnO_2:F coated glass (FTO) substrate, as the counter electrode, and a polysulfide electrolyte. (b) A conceptual schematic of the $CuInS_2$-QDs/CdS heterostructure on the TiO_2

surface. The inset illustrates the particle-packing network of a CdS film without the $CuInS_2$ QD pillars. Note that coating ZnS to finalize the SILAR deposition is important for passivating the light-absorbing $CuInS_2$-QDs/CdS sensitizers. (c) A schematic showing the relative band energy levels for charge transfer in the TiO_2/$CuInS_2$-QDs/CdS/ZnS electrode. ZnS is included because the function of ZnS coating is to passivate the sensitizers.

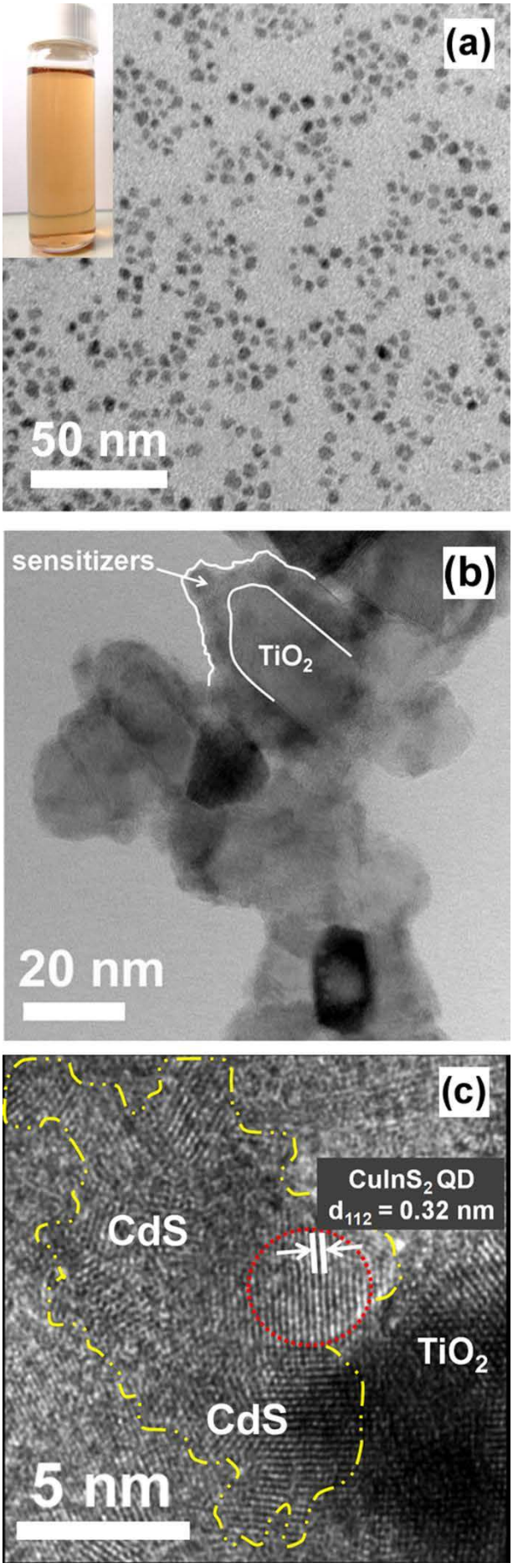
(a)
50 nm
sensitizers
(b)
TiO_2
20 nm
(c)
$CuInS_2$ QD
d_{112} = 0.32 nm
CdS
TiO_2
CdS
5 nm

Fig. 2. (a) TEM image of the as-prepared $CuInS_2$ QDs grown at 110 °C for 1 h. Inset shows the oleylamine-capped $CuInS_2$-QDs/hexane dispersion, with color of orange. (b) TEM image of TiO_2 nanocrystals sensitized with $CuInS_2$-QDs/CdS. (c) HRTEM image of TiO_2/$CuInS_2$-QDs/CdS composite. The $CuInS_2$ QDs and CdS sensitizers are encompassed by red and yellow lines, respectively.

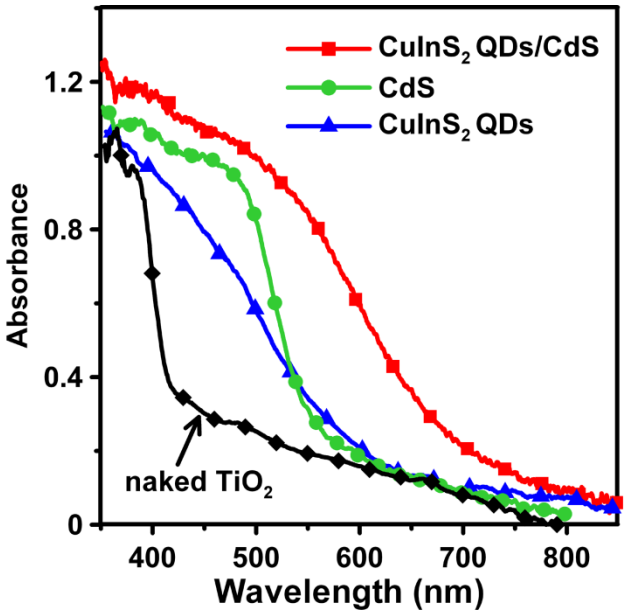

Fig. 3. Optical absorption spectra of the naked nanocrystalline TiO_2 film, and the TiO_2 films sensitized with $CuInS_2$ QDs, CdS, and $CuInS_2$-QDs/CdS.

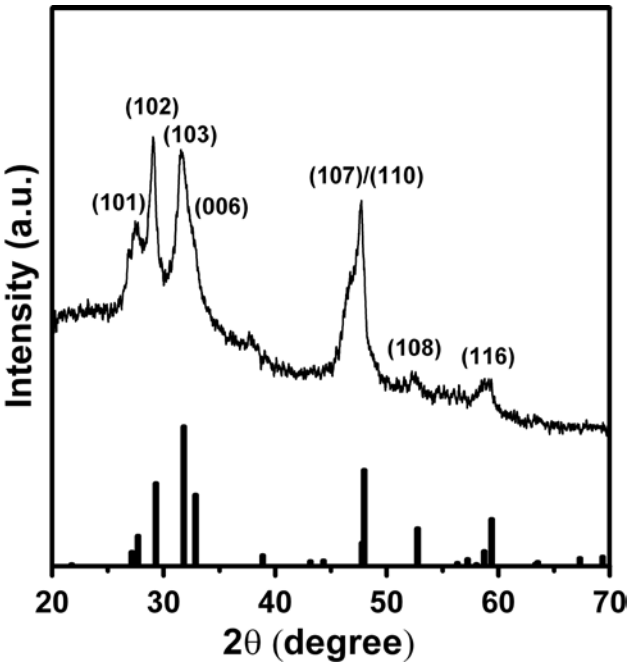

Fig. 4. X-ray diffraction (XRD) pattern of the 4-cycle SISCR CuS film indexed to the pure hexagonal phase. The standard pattern of CuS (JCPDS file no. 79-2321) is provided at the bottom.

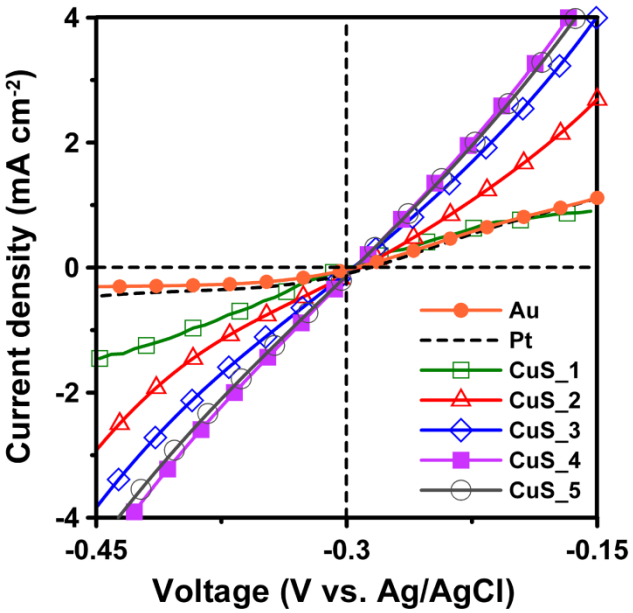

Fig. 5. Potentiostatic current–voltage polarization curves of the Pt and Au electrodes and the CuS electrodes from varying SISCR cycles in the polysulfide electrolytes.

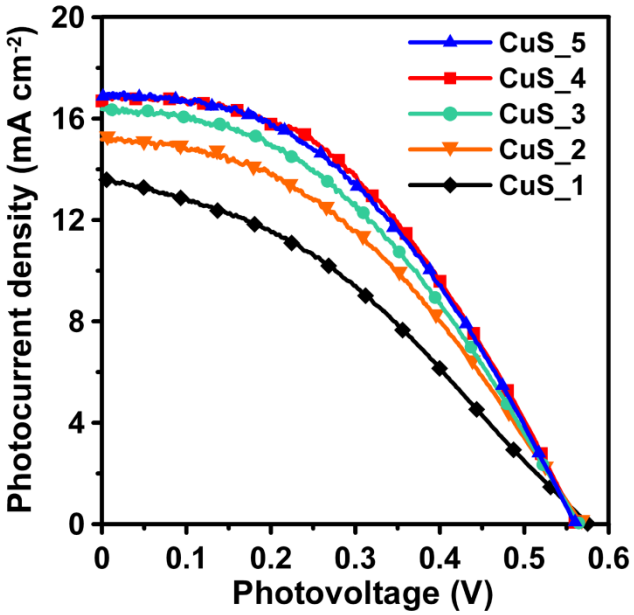

Fig. 6. Photocurrent–voltage characteristics of QDSSCs assembled with the TiO_2/$CuInS_2$-QDs/CdS/ZnS photoanode and the CuS counter electrodes from varying SISCR cycles under AM1.5-type solar illumination at 100 mW cm^{-2}.

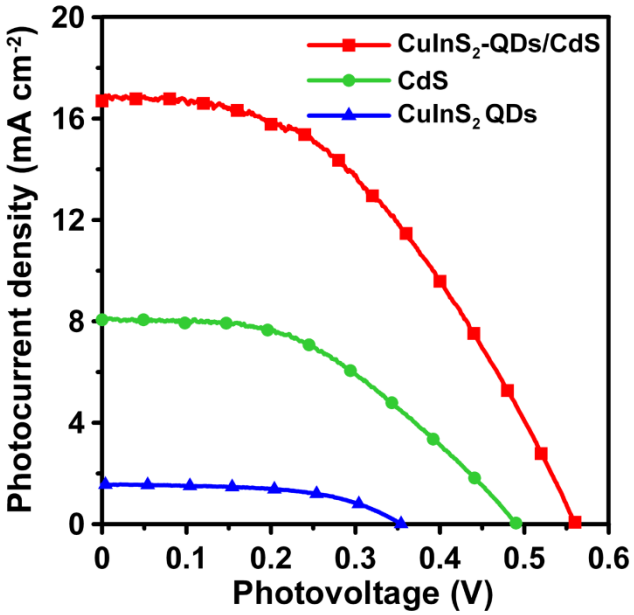

Fig. 7. Photocurrent–voltage characteristics of QDSSCs assembled with the 4-cycle SISCR CuS counter electrode and various photoanodes including the electrodes sensitized with $CuInS_2$-QDs, CdS, and $CuInS_2$-QDs/CdS, all coated with a final ZnS layer, under AM1.5-type solar illumination at 100 mW cm^{-2}.

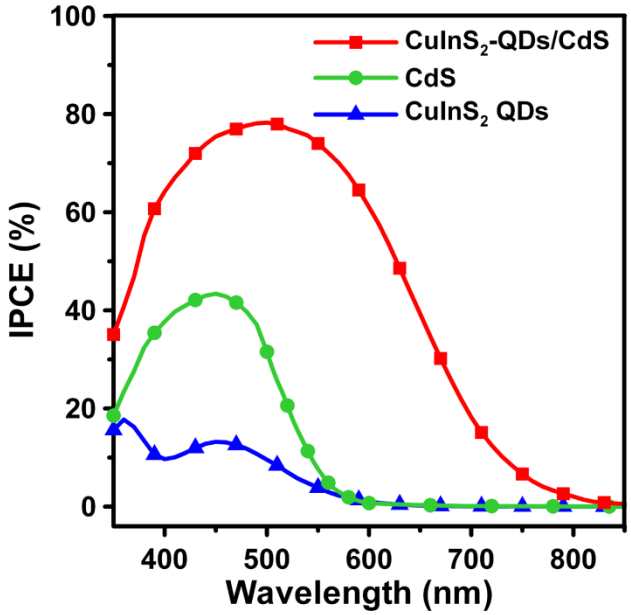

Fig. 8. IPCE spectra of QDSSCs assembled with the 4-cycle SISCR CuS counter electrode and various photoanodes including the electrodes sensitized with $CuInS_2$-QDs, CdS, and $CuInS_2$-QDs/CdS, all coated with a final ZnS layer, measured as a function of incident light wavelength.

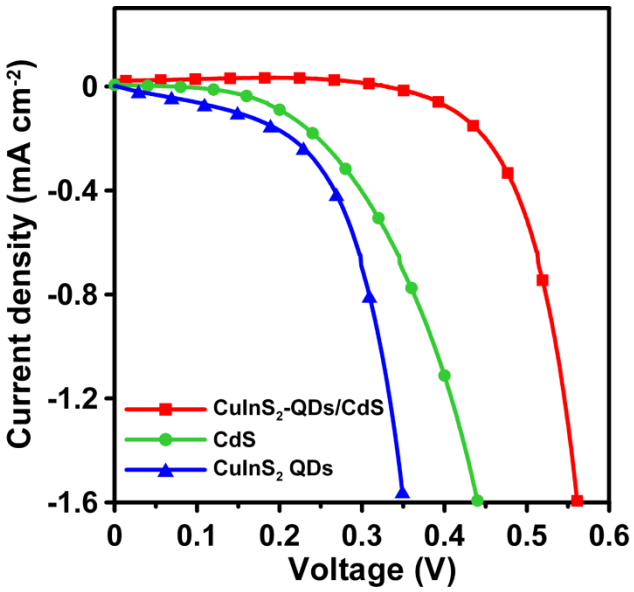

Fig. 9. Dark current–voltage characteristics of QDSSCs assembled with the 4-cycle SISCR CuS counter electrode and various photoanodes including the electrodes sensitized with $CuInS_2$-QDs, CdS, and $CuInS_2$-QDs/CdS, all coated with a final ZnS layer.

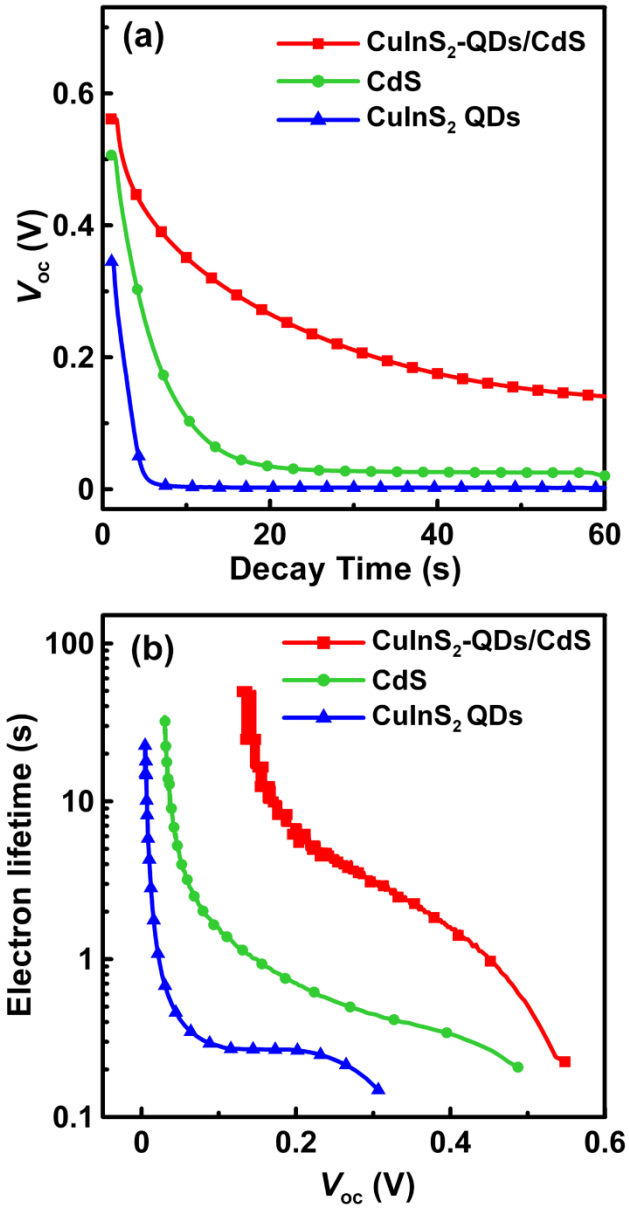

Fig. 10. (a) The variation of open-circuit voltage (V_{oc}) decay with time and (b) the dependence of electron lifetime on V_{oc} for QDSSCs assembled with the 4-cycle SISCR CuS counter electrode and various photoanodes including the electrodes sensitized with $CuInS_2$-QDs, CdS, and $CuInS_2$-QDs/CdS, all coated with a final ZnS layer. The QDSSCs were illuminated at 100 mW cm^{-2} before measuring the V_{oc} decay in the dark.